Available online at www.sciencedirect.com
SCIENCE DIRECT®
Journal of Power Sources 140 (2005) 217–225
JOURNAL OF POWER SOURCES
www.elsevier.com/locate/jpowsour

A study of Ni + 8YSZ/8YSZ/$La_{0.6}Sr_{0.4}CoO_{3-\delta}$ ITSOFC fabricated by atmospheric plasma spraying

R. Zheng*, X.M. Zhou, S.R. Wang, T.-L. Wen, C.X. Ding

Shanghai Institute of Ceramics, Chinese Academy of Sciences (SICCAS), 1295 Dingxi Road, Shanghai 200050, PR China

Received 17 November 2003; received in revised form 31 May 2004; accepted 4 June 2004
Available online 19 December 2004

Abstract

An intermediate temperature solid oxide fuel cell (ITSOFC) based on 8YSZ electrolyte, $La_{0.6}Sr_{0.4}CoO_{3-\delta}$ (LSCo) cathode, and Ni − 8YSZ anode coatings were consecutively deposited onto a porous Ni-plate substrate by atmospheric plasma spraying (APS). The spray parameters including current, argon and hydrogen flow rate, and powder feed rate were investigated by an orthogonal experiment to fabricate a thin gas-tight 8YSZ electrolyte coating (80 μm). By proper selection of the spray parameters to decrease the particles velocity and temperature, the sprayed NiO + 8YSZ coating after reducing with hydrogen shows a good electrocatalytic activity for H_2 oxidation. With the same treatment, 100–170 μm dimensions LSCo particle could keep phase structure after spraying. And the deposited LSCo cathode shows a good cathode performance and chemical compatibility with 8YSZ electrolyte after operating at 800 °C for 50 h. Output power density of the sprayed cell achieved 410 mW cm^{-2} at 850 °C and 260 mW cm^{-2} at 800 °C. Electrochemical characterization indicated that IR drop of 8YSZ electrolyte, cathodic polarization, and the contact resistance at LSCo/8YSZ interface were the main factors restricting the cell performance. The results suggested that the use of APS cell allowed the reduction of the operating temperature of the SOFC to below 850 °C with lower production costs.

Keywords: ITSOFC; Atmospheric plasma spray; $La_{0.6}Sr_{0.4}CoO_{3-\delta}$ cathode

1. Introduction

In order to reduce production costs and improve long-term stability, great efforts have been made towards the development of ITSOFC. Under the reduced operation temperature, the electrolyte ohmic resistance and electrode reaction resistance of ITSOFC must be minimized to obtain high power density. The electrolyte ohmic resistance can be reduced by utilizing materials with higher ionic conductivity, such as doped CeO_2 and doped $LaGaO_3$ [1–3], or reducing the thickness of YSZ electrolyte. This study correlates with the latter case. The thin-coatings of anode, electrolyte and cathode were deposited on porous Ni-plate substrate in a consecutive APS process.

It is known that the conventional coating technologies, such as tape casting, screen printing and dip molding, have to go through a high temperature sintering process. For large area cells, this step will inevitably introduce a lot of defects, such as warp, crackle and pore. At the same time, in order to assure the electrolyte densification, the electrode porosity and good electrochemical interlamellar contact, the sintering steps would be a complex procedure. This time-consuming processes is a shortage for mass production, and is difficult to meet the strict cost targets for the successful introduction of SOFCs to the strongly competitive energy market.

The main advantage of porous metallic supported thin-coating cell fabricated by APS is to allow enlarging the cell area without sintering defects and improve its mechanical properties [4]. In addition APS easily controls the component composition and microstructure through variation of spray parameters. Comparing with other deposition techniques such as electrochemical vapor deposition (EVD) [5] and vacuum plasma spray (VPS) [6], APS does not need sophisticated apparatus and controlled atmosphere which would increase the cost of fabrication. Moreover, high material deposition rates of APS promise inexpensive and fast cell production with potential automated production lines.

Ni + 8YSZ was applied for SOFC anode. The 8YSZ component in the anode was expected to extend the effective electrolyte zone deep into the anode layer enabling oxide

* Corresponding author. Tel.: +86-21-5241-2069; fax: +86-21-5241-3903.
E-mail address: kunami@mail.sic.ac.cn (R. Zheng).

0378-7753/$ – see front matter © 2004 Elsevier B.V. All rights reserved.
doi:10.1016/j.jpowsour.2004.06.015

ions to be conveyed to the three-phase boundary (TPB) sites, and act as a supporting matrix for Ni particles ensuring their uniform dispersion and preventing their sintering.

$La_{0.6}Sr_{0.4}CoO_{3-\delta}$ (LSCo) was selected as the cathode material to reduce cathode reaction resistance. It had been considered as a candidate cathode material for ITSOFC because of its high electronic [7] and ionic conductivity [8] as well as high catalytic activity for oxygen reduction [9]. The main problem of LSCo was its vigorous reactivity with 8YSZ at over 900 °C [10]. It was expected that this problem will not be serious when the cell operating temperature is below 850 °C, and the interface reaction between 8YSZ and LSCo during preparation process is restrained by the instant melting and depositing technique of APS.

In this study, the spray parameters were optimized to obtain porous electrode and dense electrolyte. The performance of APS single cell was investigated at 700–850 °C. The cell total voltage drop was separated into ohmic and nonohmic contributions. The ohmic one was compared with the 8YSZ IR drop, which was estimated from the known conductivity and thickness of the electrolyte. The anodic and cathodic contributions to cell polarization were separated using a reference electrode. The degradation of the electrodes performance was also discussed.

2. Experimental

2.1. Preparation of spraying powders

Commercial 8YSZ (8 mol% yttria stabilized zirconia, TOSOH Corp., average particle diameter 50 μm) and Ni with 40 vol.% (SCR Chem., Shanghai, China, average particle diameter 75 μm) powders were mixed for starting anode material. The powder mixture after ball milled were calcined at 1300 °C for 5 h in air, then crushed. The particle dimension distributed was adjusted in the range of 10–60 μm for a good flowability, which is suitable for plasma spraying. Fig. 1(a) shows the morphology of the 8YSZ/NiO mixture. As it is shown, the spherical or ellipsoidal particle was 8YSZ (20–60 μm) and the irregular agglomeration was NiO (10–60 μm).

Commercial TOSOH 8YSZ powder, which has a typical granule diameter of approximately 50 μm and a primary particle size of 0.4 μm within a granule, was selected to prepare the electrolyte coating.

Cathode $La_{0.6}Sr_{0.4}CoO_{3-\delta}$ powder was prepared by conventional solid-state reaction method. Appropriate ratio of La_2O_3 (>99.95%), $SrCO_3$ (99.99%) and Co_3O_4 (95%) powders were mixed and ball milled for 24 h in ethanol. After drying, the powders were heated at 1000 °C for 3 h in air. Calcined powders were again ball milled and pressed into pellet. The pellet were sintered at 1300 °C for 3 h in air. X-ray powder diffraction (Rigaku D/Max rB) shows that the obtained sintered pellet was a single phase of LSCo without any impurities. The sintered LSCo pellets were crushed, and superior particle size (100–170 μm) were selected in order to ensure good flowability and phase stability during APS which was attributed to mainly surface melt. The morphology of the LSCo powder is shown in Fig. 1(b).

2.2. Preparation of the cell

The plasma spray process was based on the generation of a plasma jet consisting of argon or argon/hydrogen admixture, which was ionized by a high current to from a plasma torch. The powders to be sprayed were injected into the plasma jet where they were accelerated, melted and finally deposited onto the substrate. The coating was formed by flattening and solidification of the particles at impact on the substrate. Therefore, the particle temperature and velocity at the point of impact would determine the coating microstruc-

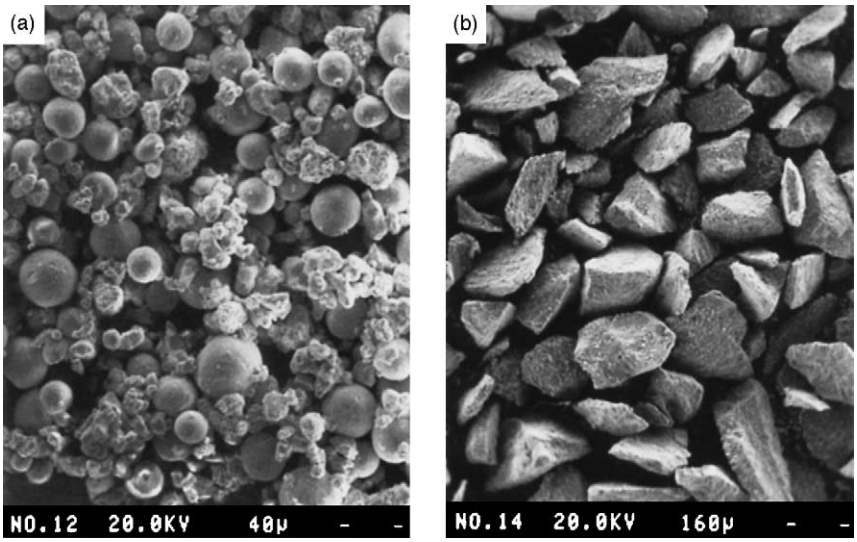

Fig. 1. Powders used for the fabrication of the SOFC: (a) NiO + 8YSZ; (b) LSCo.

ture. For a given particle morphology and dimension distribution, particle trajectory within the plasma jet determined its temperature and velocity. We investigated the current, argon and hydrogen flow rate, and powder feed rate to control the coating microstructure.

The plasma spraying was carried out with a Metco A-2000 atmospheric plasma spraying equipment (Sulzer Metco AG, Switzerland). Argon gas was the primary plasma gas, and hydrogen gas was used as the secondary gas. The whole spray processes all adopted conventional conical F4MB nozzles (6 mm in diameter). The powders were fed with Twin-System (Plasma-Technick AG, Switzerland). The anode, electrolyte and cathode coatings were deposited consecutively on a porous Ni-plate substrate (CERIS, Beijing, China), which was about 1.5 mm in thickness and had an interconnecting porosity beyond 45 vol.%.

2.2.1. Deposition of the Ni + 8YSZ cermet anode coating

Previous researches showed that the two-phase anode coating should have a continuous network structure of both Ni and 8YSZ components in order to have the minimum resistance, good electrocatalytic activity for H_2 oxidation, and rich three-phase boundary (TPB) sites as well as good adherence to the electrolyte [11]. Therefore, in this study, NiO and 8YSZ particles were of similar size and the Ni content was fixed at 40 vol.%. In order to restrain the Ni evaporation, the Ni was sprayed as the NiO powder. And the reduction of NiO by hydrogen to Ni at cell operating condition would lead to a further increase in porosity which ensured sufficient TPB sites in the anode. Before spraying, the Ni-plate substrate surface was coarsened by SiC particle (0.1 mm) on sheet glass in order to improve the interface combination between NiO + 8YSZ and Ni-plate. Then the Ni-plate was degreased ultrasonically in acetone. The NiO and 8YSZ mixture powders were sprayed with the optimized parameters which were listed in Table 1. The minor current, argon flow rate, hydrogen flow rate, and superior powder feed rate, spray distance yielded a decrease in both particle velocity and temperature [12]. It was desired for the porous anode coating.

2.2.2. Deposition of the 8YSZ electrolyte coating

For improving the APS cell performance, it is necessary to spray a gas-tight electrolyte coating as thin as possible.

Table 1
Atmospheric plasma spraying parameters for the single cell

Spray parameter	Anode	Electrolyte	Cathode	Unit
Torch current	500	660	500	A
Primary plasma gas flow (Ar)	35	42	50	slpm[a]
Secondary plasma gas flow (H_2)	10	15	6	slpm
Powder feed rate	20	18	27	g min^{-1}
Spray distance	110	100	130	mm

[a] Standard liters per minute.

Table 2
The factors investigated and their ternary levels

Factor		Level 1	Level 2	Level 3	Unit
C	Current	630	660	690	A
A	Argon flow rate	42	45	48	slpm
H	Hydrogen flow rate	12	15	18	slpm
P	Powder feed rate	14	16	18	g min^{-1}

It is only achievable when completely molten 8YSZ particles were compactly flattened and solidified without defects during impacting on the substrate. Therefore, 8YSZ particles with high temperature and velocity are desired. The higher particle temperature mainly depended on a longer dwell time of the plasma, while the higher velocity would decrease the dwell time. Therefore, the spray parameters must be optimized to give attention to both temperature and velocity.

An orthogonal experiment was designed to investigate how the spray gun parameters, namely, current (*C*), argon flow rate (*A*), hydrogen flow rate (*H*), and powder feed rate (*P*), influenced the 8YSZ coating density. The ranges of spray parameters were chosen to vary around a standard production setting for producing a dense ZrO_2 coating. These different parameters and their ranges were given in Table 2. The orthogonal experiment was designed as a $L_9(4^3)$ design, each of the four factors having three levels and there being nine treatments altogether. The design matrix was given in Table 3, the numbers there denoting the level value of factors *C*, *A*, *H*, and *P* according to the figures were shown in Table 2. After sprayed, the cross-section of 8YSZ coating was polished with diamond paste (up to 0.04 μm) to obtain flat and smooth surface. Its porosity, measured by quantitative image analysis, was chosen as reference point for coating density.

In order to observe the natural fracture surface microstructure, another 8YSZ coating was sprayed on NiO/8YSZ cermet flake (the coating on Ni-plate substrate could not be cleaved without damage).

Table 3
The $L_9(4^3)$ design matrix

Treatment	Parameters of the orthogonal experiments				Coating porosity (%)
	C	*A*	*H*	*P*	
1	1	1	1	1	8.97
2	1	2	2	2	10.45
3	1	3	3	3	15.10
4	2	1	2	3	3.67
5	2	2	3	1	6.04
6	2	3	1	2	14.83
7	3	1	3	2	4.77
8	3	2	1	3	6.98
9	3	3	2	1	10.21

2.2.3. Depositing of the LSCo cathode coating

The sprayed parameters of LSCo cathode were optimized in a similar way as the anode. It should be mentioned that the perovskite cathode tended to decompose, especially in the case when hydrogen was added to the plasma gas. Therefore, minor current and hydrogen flow rate were adopted to effectively decrease the temperature of plasma jet, and superior argon flow rate and powder feed rate were applied to shorten the particle dwell time in the plasma. Both of them would decrease the temperature of LSCo particle [12]. In addition to the superior particle size, surface molten LSCo particle was expected to be sprayed without decomposition. The optimized parameters were listed in Table 1. Before testing, sprayed LSCo cathode coating was heat-treated in air at 800 °C for 2 h. The phase structure of LSCo coatings before and after heat-treatment were analyzed by X-ray diffractometer.

2.2.4. Measurement of coating's chemical composition

In order to check whether some changes of chemical composition would take place during deposition and formation of coatings by APS, the element constituents of the pelletized granules and the powders scraped from deposited NiO + 8YSZ, 8YSZ, and LSCo coatings were measured by ICP-AES (Varian AX, America).

2.3. Characterization of the cell

The construction of testing set for the APS cell based on Ni-plate substrate is shown schematically in Fig. 2. The effective working area of the single cell was considered as equal to the cathode area (0.512 cm^2). Pt wires were fixed to LSCo cathode and Ni-plate substrate with platinum paste. Before testing, the anode was fully reduced in H_2 atmosphere at 800 °C for 2 h. H_2 (saturated by water at ambient temperature) passed through the anode chamber with a flow rate of 15 ml min^{-1} while O_2 (20 ml min^{-1}) was supplied to the cathode side.

The *I–V* and *I–P* curves were measured with four-probe method by an electrochemical workstation (model IM6e, Zahner-Elektrik GmbH, Germany) over the temperature range of 700–850 °C with an accuracy of ±1 °C. The electrode polarization curves was estimated by the following equation [13]

$$\eta = E - IR_b \quad (1)$$

where I is the applied current between the working electrode and the counter electrode; E the voltage between the working electrode and the reference electrode; R_b the ohmic resistance estimated from the alternating current (ac) impedance data. The ac impedance spectroscopy was observed with four-probe technique under open circuit condition. The frequency range was 1 MHz to 1 Hz, and in some cases down to 0.1 Hz. The measured impedance spectra were fitted by using a nonlinear least square fitting computer program.

Morphological evolution of the cell coatings were traced by taking SEM photographs (S570 HITACHI, Japan) in each step of the APS fabrication. After the cell tests, the microstructure of the sprayed cell cross-section and the elemental distribution near the LSCo/8YSZ interface were observed by using an electron probe microanalyzer (EPMA-8705QH_2).

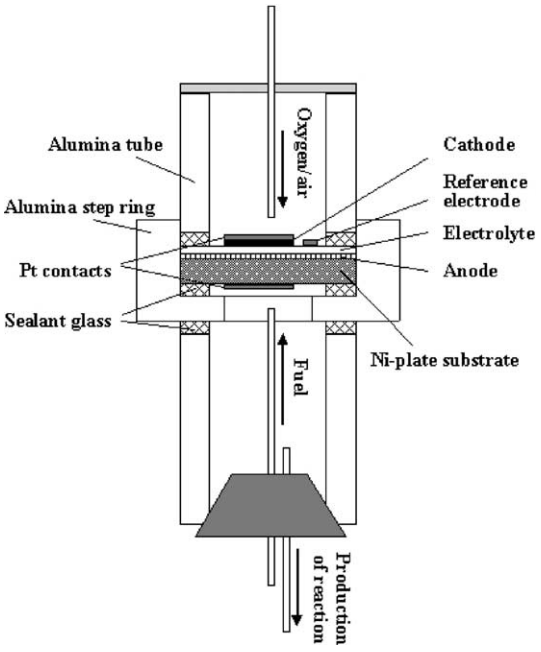

Fig. 2. The scheme of the testing APS cell system.

3. Results and discussion

3.1. Structural characterization of APS cell

3.1.1. NiO + 8YSZ cermet coating

Fig. 3 shows the surface and cross-section of sprayed NiO + 8YSZ cermet coating. The results in Fig. 3(a) indicated the 8YSZ particles whose surface was coated with NiO were soldered around the surface. Completely molten NiO particles were filled in the gap of 8YSZ network structure or wrapped on the surface of 8YSZ particles. Because the 8YSZ particles had formed a network structure, they would effectively act as a supporting matrix for Ni particles ensuring their uniform dispersion and preventing Ni (after reduction) from sintering during cell operating. Fig. 3(b) shows the cross-section of polished NiO + 8YSZ/8YSZ coatings. Since formed a good component gradient, the anode compactly combined with 8YSZ electrolyte. The ICP-AES results (Table 4) shows a little increase of nickel content which may be caused by NiO partly deoxidized to Ni during spraying. The relative proportion between zirconium and yttrium was basically kept stable.

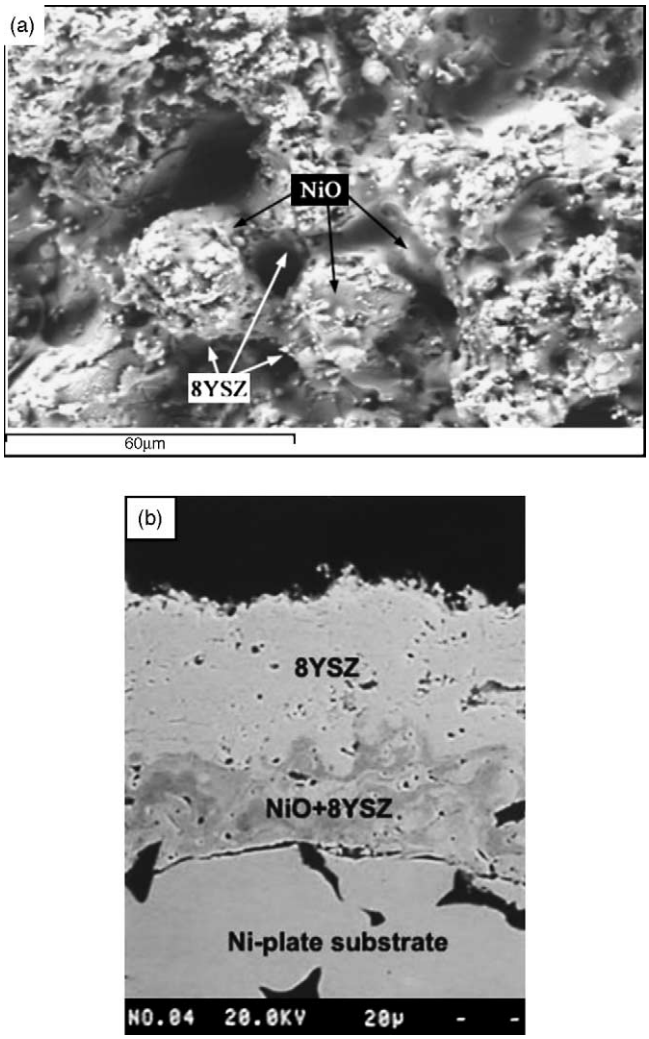

Fig. 3. Surface (a) and cross-section (b) of sprayed NiO + 8YSZ coating on Ni-plate substrate.

3.1.2. 8YSZ electrolyte coating

The results of the orthogonal experiment were shown in Table 3. The variance analysis indicated that the significant difference of spray parameters in the chosen ranges obeyed the following relationship: argon flow rate > current > hydrogen flow rate > powder feed rate. The optimized parameters were listed in Table 1. Fig. 3(b) shows the 8YSZ coating (60–70 μm) sprayed with the optimized parameters exhibited a dense lamellar microstructure. The cross-section pore mainly was closed pore and porosities were in the range of 3.5–4 area%. It seems to be an ideal structure for the gas-tight electrolyte coating. However, the electrochemical experiment shows that the cell open circuit voltage always could not achieve the ideal value unless the 8YSZ coating thickness was beyond 150 μm. So the natural fractures surface of sprayed 8YSZ coating was investigated (Fig. 4(a)).

SEM image of the 8YSZ coating after fracture revealed that most granule of TOSHO powder was crushed by plasma jet, the primary particle was completely melted and the subsequent condensation layer exhibited a typical lamellar splat structure. A lamella deposited by each spray scanning was about 4.5–6 μm thick, there were 3–4 splat layers in each lamella and the thickness of a splat layer was about 1.5–2 μm (Fig. 4(a)). When the surface temperature of the substrate [14] or the previously deposited layer [15] was higher than 2000 °C, the thermal contact resistance between the splat and the under layer was lower than 10^{-7} K m^2 W^{-1}. The cooling of the splat, just after flattening, was very fast (>10^7 K s^{-1}), resulting in a columnar structure within the splat. However, the coating exhibited poor contact between the successive lamella, some welding micro-crack (diameter below 0.5 μm) was observed. If the column growth of the new impacting splat could extend to the columns of the already solidified one, the combination between these lamellas would be improved. Unfortunately, it could not be achieved unless the surface temperature of the splat upon impact of the next splat was higher than 2000 K (temperature determined by the calculation of Vardelle et al. [16]). Moreover, some obvious crack (diameter nearly 0.5 μm) appeared in the coating surface (Fig. 4(b)) which might be caused by the residual stresses generated upon cooling between the successive lamellas. All of these defaults caused some gas permeable leakage when the 8YSZ coating thickness is thinner than 150 μm. Adding some particle with high temperature vitreous phase in 8YSZ powder [17] or using an excimer laser to remelt the surface crack [18] might be helpful to fabricate gas-tight 8YSZ electrolyte coating.

The chemical composition of deposited 8YSZ electrolyte coating was listed in Table 4. There were some element loss of both zirconium and yttrium, it may be related to volatilization during spraying. However, the relative element's proportion was basically kept stable.

Table 4
The chemical composition of deposited coatings by ICP-AES (wt.%)

	NiO + 8YSZ			8YSZ		$La_{0.6}Sr_{0.4}CoO_{3-\delta}$		
	Ni	Zr	Y	Zr	Y	La	Sr	Co
Designed	44.1	28.1	4.78	63.03	11.7	38.07	16	26.92
Before spray	44.62	28.44	5.10	63.79	12.85	36.99	15.55	26.15
After spray	47.32	27.52	4.76	62.47	10.85	35.24	15.45	22.67

3.1.3. LSCo cathode coating

Fig. 5 shows the X-ray diffraction patterns of the LSCo powder (before plasma spraying) as well as the deposited LSCo coatings before and after heat treatment, respectively. The Fig. 5(a) indicated that the as-synthesized LSCo powder was single phase of orthorhombic perovskite structure. After spraying, although XRD peaks were noticeably broader, only the orthorhombic perovskite structure was identified in Fig. 5(b). And the broadening of XRD peaks evidently become broader with a increase in the volume fraction of melted particles. After being held at 800 °C for 2 h, the XRD pattern of LSCo coating in Fig. 5(c) was identical with that of as-synthesized LSCo powder. The SEM photograph of

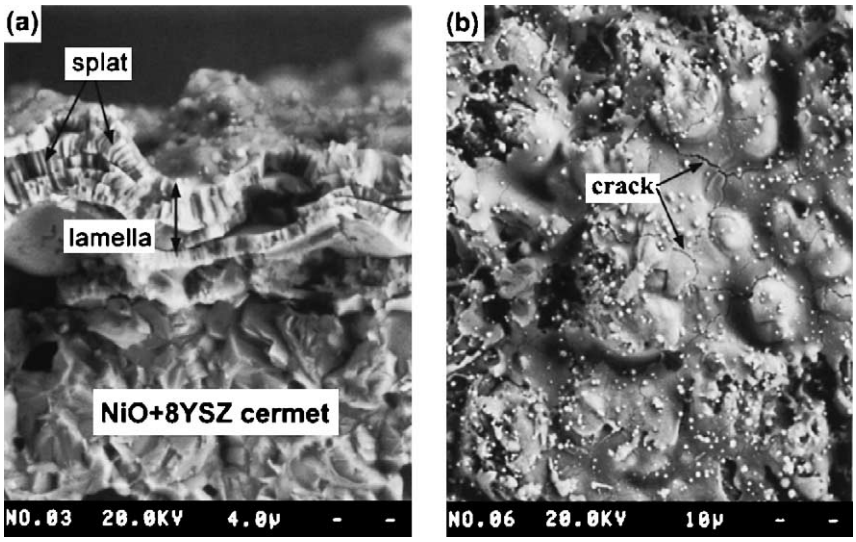

Fig. 4. Cross-section and surface of 8YSZ coating on NiO/8YSZ cermet flake.

coating surface shows that the coating mainly consisted of the surface melted LSCo particles (Fig. 6). And its surface morphology basically did not change from that before heat treatment. The present results indicated that the broadening of XRD was presumably caused by microstrain of the melted parts [19]. The ICP-AES results (Table 4) shows that there were some element loss for cobalt compared with lanthanum and strontium. The following electrochemical experiments shows that this trivial element loss would not evidently influence LSCo performance. With the optimized spray parameters, the LSCo coating could keep its phase structure without decomposition. And it shows good chemical stability with 8YSZ electrolyte, this would be discussed later.

3.2. Electrochemical characterization of APS cell

The temperature dependence of the sprayed cell performance in the range of 700–850 °C with hydrogen and oxygen as operating gases can be seen from the typical *i–V* and *i–P* curves shown in Fig. 7. The OCV was close to 0.95 V.

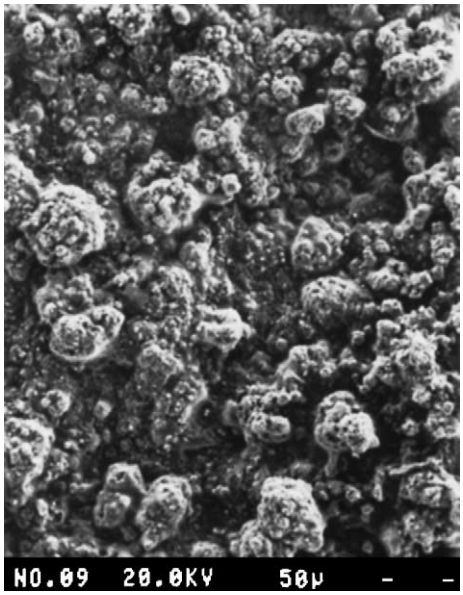

Fig. 6. Surface of LSCo coating before heat treatment.

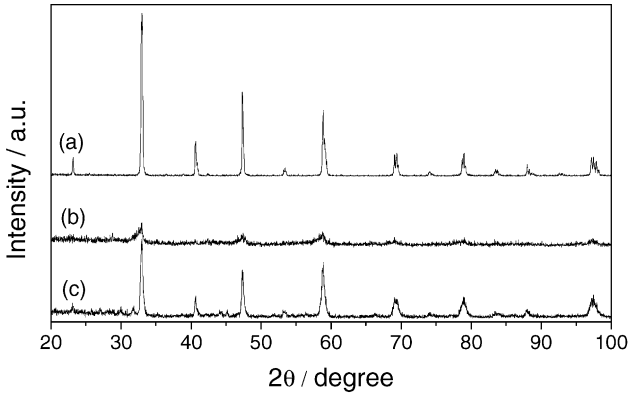

Fig. 5. XRD patterns of LSCo powder and coating: (a) synthesized powder; (b) coating without heat treatment; (c) coating after heat treatment.

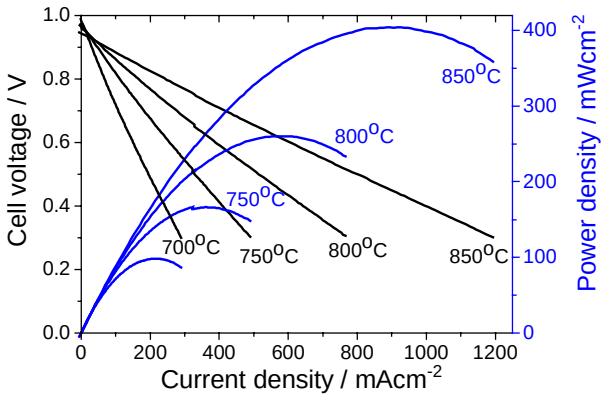

Fig. 7. Performance of APS cell with H_2/O_2 as operating gases.

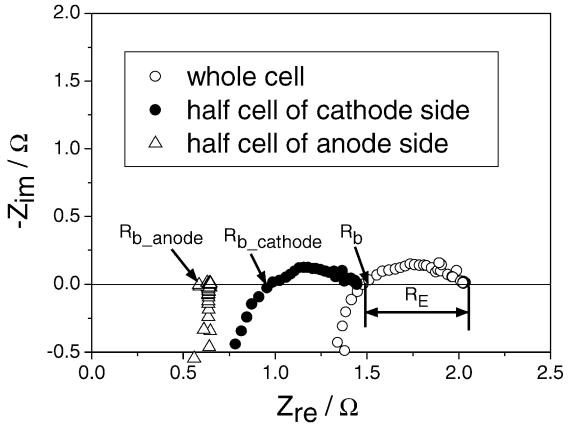

Fig. 8. Cole–Cole plots of sprayed cell under open circuit condition at 800 °C.

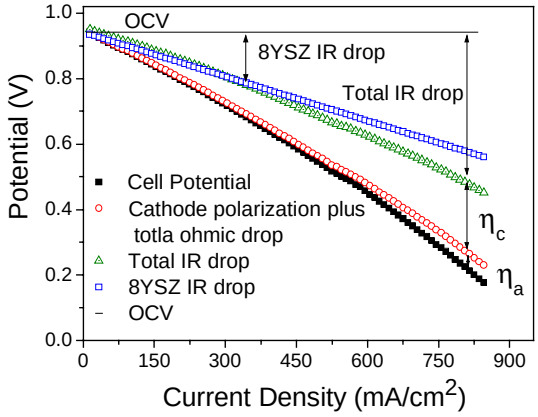

Fig. 9. Separation of cell polarization components at 800 °C.

The power density at a cell voltage of 0.5 V decreased from approximately 390 mW cm^{-2} at 850 °C to 250 mW cm^{-2} at 800 °C, to 160 mW cm^{-2} at 750 °C, and to 100 mW cm^{-2} at 700 °C. The use of LSCo as the cathode powder led to a maximum power density of about 405 mW cm^{-2} at 850 °C, which was an excellent initial performance for nearly 0.1 mm thick 8YSZ electrolyte.

The Cole–Cole plots of ac impedance spectroscopy for the sprayed cell was depicted in Fig. 8, combined with those of anodic and cathodic half-cell. The intercepts on the real impedance axis at high frequency for the whole and half-cell correspond to the R_b ($R_{b\_cathode}$ and R_{b_anode}), which indicated the ohmic resistance including electrolyte resistance and interface contact resistance. According to Eq. (1), the electrode polarization at 800 °C were estimated. The difference between intercepts on real impedance axis at low and high frequencies for the electrode impedance arc was electrode reaction resistance (R_E). The R_E for the cathode was approximate 0.52 Ω cm^{-2}, while for the anode was only 0.024 Ω cm^{-2} at 800 °C. The lack of a "pore forming process" led to a lower overall porosity in the LSCo cathode in comparison to the anode (Fig. 14(a)), the anodic oxidation reaction shown a lower reaction resistance than cathodic reduction reaction.

Fig. 9 shows the voltage drop versus current density for the APS cell at 800 °C. The total voltage drop was separated into ohmic and nonohmic contributions. The use of a reference electrode allowed separation of anodic and cathodic contributions to the cell polarization. 8YSZ IR drop was estimated with the following equation:

$$R_{\text{bulk}} = \frac{l}{\sigma \times A} \quad (2)$$

where σ represents the 8YSZ conductivity at 800 °C [20], A the effective cell working area and l the 8YSZ coating thickness. The results in Fig. 10 indicated that the polarization of the electrodes ($\eta_a + \eta_c$) account for about 30% of the total voltage drop at 500 mA cm^{-2}. The cathodic polarization (η_c) was larger than the anodic polarization (η_a) which was almost negligible for current density below 600 mA cm^{-2}. The 8YSZ electrolyte IR drop represented about 60% of the total voltage drop. The ohmic loss across the 80 μm 8YSZ electrolyte coating was one of the main factors which restricted the spray cell performance. The remainder of the ohmic drop about 10% of the total voltage drop was considered mainly due to contact resistance at the LSCo/8YSZ interface. SEM photograph of the cross-section of spray cell (Fig. 14(a)) shows a distinct boundary at LSCo/8YSZ interface, which may be due to the mismatch in thermal expansion coefficient between LSCo and 8YSZ. As a result it could be the reason for the larger cathodic contact resistance.

The voltage drop of the different cell components at different operating temperature were evaluated in Fig. 10. If fuel could be recycled at SOFC operating condition, compared with energy conversion efficiency (ECE), the fuel utilization efficiency (FUE) is not so important. Therefore, we selected a voltage of 0.5 V as the reference point which approximately corresponded to the maximum ECE at different operating temperatures. The current density at the 0.5 V cell voltage decreased from approximately 780 mA cm^{-2} at 850 °C to 500 mA cm^{-2} at 800 °C, 310 mA cm^{-2} at 750 °C, and 180 mA cm^{-2} at 700 °C. The results in Fig. 10 indicated that

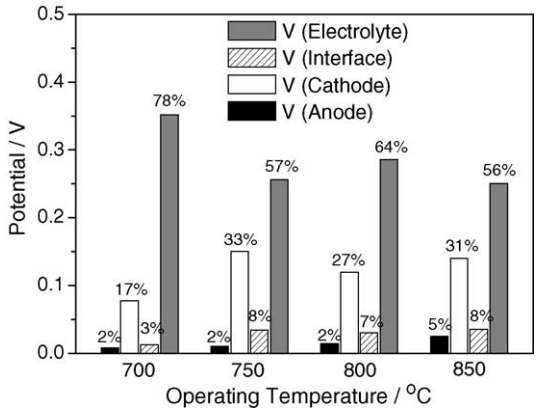

Fig. 10. The voltage loss of the components of the APS cell with H_2/O_2 as operating gases at 0.5 voltage as a function of temperature.

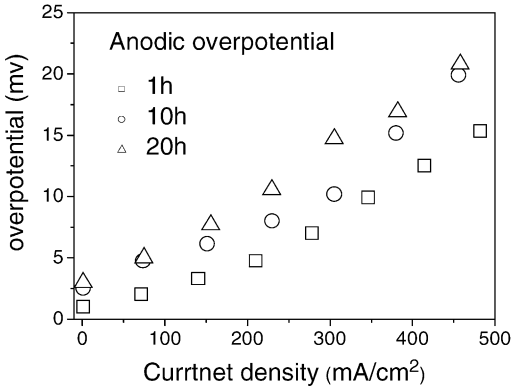

Fig. 11. The electrode overpotential variations against operation time at 850 °C.

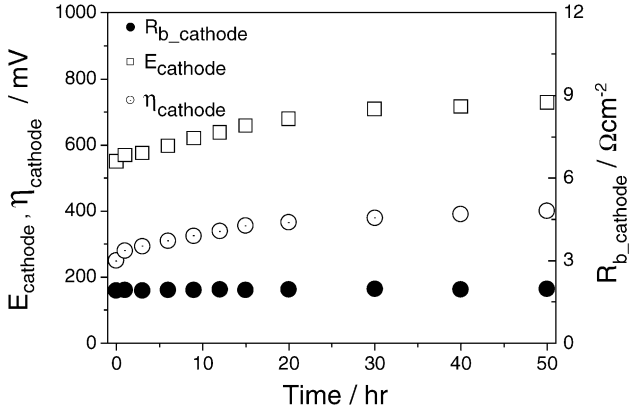

Fig. 12. LSCo cathode performance at current density of 500 mA cm^{-2} at 800 °C.

the voltage drop of the maximum ECE above 750 °C were nearly same proportion: electrolyte ohmic resistance 60%, cathode reaction resistance 30%, LSCo/8YSZ interface contact resistance 7%, and anode reaction resistance 3%.

Further improvement of the cell performance could be achieved by reducing the thickness of 8YSZ electrolyte film, modifying the cathode microstructure, and improving the combination on the LSCo/8YSZ interface.

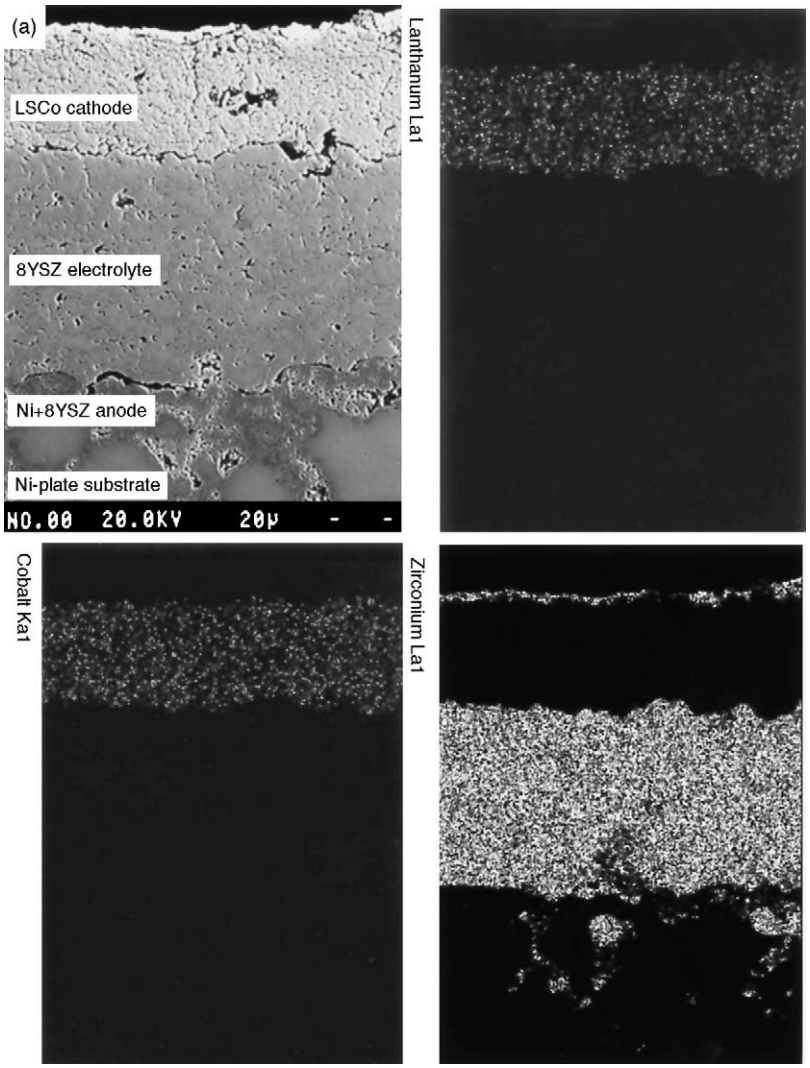

Fig. 13. EPMA analysis results: (a) SEM of the cross-section of spray cell at 800 °C for 50 h, La, Co, and Zr distributions.

3.3. Electrode stability of APS cell

The electrode degradation was a main factor that influences the stability of APS cell at high temperatures. Ni sintering and LSCo/YSZ reaction, which form the oxide ion insulator products such as $La_2Zr_2O_7$ and $SrZrO_3$ [21], have been proposed to be the most important factors, respectively, for anode and cathode degradation. Therefore, the electrode overpotential variations against operation time were studied at 800 and 850 °C. It was shown in Fig. 11 that the anode overpotential nearly did not increase even when the cell was held at 850 °C for 20 h. The results suggested that sprayed 8YSZ continuous network structure successfully restrained the Ni sintering.

However, the obvious cathodic degradation was observed after the cell was held at 850 °C for over 20 h. The cathode overpotential increased from 150 to 250 mV at a current density of 500 mA cm^{-2}. Although obvious reaction layer did not be observed, we found that the center of strontium distribution within LSCo cathode slightly shifted to 8YSZ electrolyte side. We considered that there still had some strontium diffusion into LSCo/8YSZ interface which caused the increasing of cathode polarization. In order to avoid this problem the cell operating temperature was reduced to 800 °C. The LSCo cathode polarization shows a moderate increasing under a constant current density of 500 mA cm^{-2} at 800 °C for 50 h (Fig. 12). The increase in polarization was mainly due to an increase in η while the change in $R_{b\_cathode}$ was negligible.

The EPMA micrograph in Fig. 13 shows the microstructure of the sprayed cell's cross-section and its corresponding elements distribution. The results shows that the profile of all elements distributions were all identical with the chemical constitution of the corresponding coatings. It indicated that the chemical composition of deposited coatings could keep stable at 800 °C for 50 h.

4. Conclusions

With the optimized APS parameters, thin coating cell based on 80 μm 8YSZ electrolyte, LSCo cathode, and Ni + 8YSZ cermet anode was fabricated, and it shows an excellent performance with maximum power density of 410 mW cm^{-2} at intermediate temperature of 850 °C. From the XRD and EPMA results, the LSCo coating could keep stable phase component after APS and retain chemical compatibility with 8YSZ electrolyte after operating at 800 °C for 50 h. The 8YSZ electrolyte IR drop, cathodic polarization, and the contact resistance at the LSCo/8YSZ interface were the main factors restricting the cell performance. The present research suggested that the use of APS cell allowed the reduction of the operating temperature of the SOFC to below 800 °C with low production costs.

Acknowledgements

This research was financially supported by Development for High Technology under contract number (2002AA517010) and Sino-German Center for Scientific Research Foundation with project number GZ219(101/17). The authors express deep thanks for their supports.

References

[1] K. Echuchi, T. Setoguchi, T. Inoue, H. Arai, Solid State Ionics 52 (1992) 165–172.
[2] K. Kuroda, I. Hashimoto, K. Adachi, J. Akikusa, Y. Tamou, N. Komada, T. Ishihara, Y. Takita, Solid State Ionics 132 (2000) 199–208.
[3] K. Huang, R.S. Tichy, J.B. Goodenough, J. Am. Ceram. Soc. 81 (10) (1998) 2565–2585.
[4] S. Takenoiri, N. Kadokawa, K. Koseki, J. Thermal Spray Technol. 9 (3) (2000) 360–363.
[5] Y.S. Lin, L.G.J. De Haart, K.J. De Vries, A.J. Burggraaf, in: S.C. Singhal (Ed.), Proceedings of the First International Symposium on SOFCs, Hollywood, FL, The Electrochemical Society, Pennington, NJ, October 1989, p. 67.
[6] M. Lang, R. Henne, S. Schaper, G. Schiller, J. Thermal Spray Technol. 10 (4) (2001) 618–625.
[7] J. Mizusaki, J. Tabuchi, T. Matsuura, S. Yamauchi, K. Fucki, J. Electrochem. Soc. 136 (1989) 2082.
[8] S. Sekido, H. Tachibana, Y. Yamamura, T. Kambara, Solid State Ionics 37 (1990) 253.
[9] S. Wang, T. Kato, S. Nagata, T. Honda, T. Kaneko, N. Iwashita, M. Dokiya, Solid State Ionics 146 (2002) 203–210.
[10] H.Y. Tu, Y. Takeda, N. Imanishi, O. Yamamoto, Solid State Ionics 117 (1999) 277.
[11] C.H. Lee, H.Y. Lee, S.M. Oh, Solid State Ionics 98 (1997) 39–48.
[12] M. Friis, P. Nylen, C. Parsson, J. Wigren, J. Thermal Spray Technol. 10 (2) (2001) 301–310.
[13] T. Horita, K. Yanaji, N. Sakai, H. Yokokawa, A. Weber, E.I. Tiffee, J. Electrochem. Soc. 148 (5) (2001) A456–A462.
[14] M. Vardelle, A. Vardelle, A.C. Leger, P. Fauchais, D. Gobin, J. Thermal Spray Technol. 4 (1) (1995) 50–58.
[15] P. Fauchais, M. Vardelle, A. Vardelle, L. Bianchi, A.C. Leger, Plasma Chem. Plasma Process. 16 (1) (1996) 99S–125S.
[16] M. Vardelle, A. Vardelle, P. Fauchais, J. Thermal Spray Technol. 2 (1) (1993) 79–92.
[17] P.D. Harmsworth, R. Stenens, J. Mater. Sci. 27 (1992) 611–615.
[18] Z. Liu, Appl. Surf. Sci. 186 (2002) 135–139.
[19] H.P. Klug, L.E. Alexander, X-ray Diffraction Procedures, Wiley, New York, NY, 1966, 138 pp.
[20] N.Q. Minh, T. Takahshi, Science and Technology of Ceramic Fuel Cells, Elsevier, Netherlands, 1995, 81 pp.
[21] O. Yamamoto, Y. Takeda, R. Kanno, M. Noda, Solid State Ionics 22 (1987) 241.